ACS SENSORS

pubs.acs.org/acssensors

Article

Aptamer-Functionalized Carbon Nanotube Field-Effect Transistor Biosensors for Alzheimer's Disease Serum Biomarker Detection

Hong Chen,[‖] Mengmeng Xiao,*[,‖] Jianping He, Yang Zhang, Yuqi Liang, Haiyang Liu, and Zhiyong Zhang*

Cite This: *ACS Sens.* 2022, 7, 2075−2083

Read Online

ACCESS | Metrics & More | Article Recommendations | Supporting Information

ABSTRACT: Blood-biomarker-based tests are highly important for the early clinical diagnosis of Alzheimer's disease (AD) and the treatment and care of AD patients, but the complex serum environment and extremely low abundance of AD blood protein biomarkers present challenges. Nanomaterials are promising for constructing highly sensitive transistor-based biosensors due to their small size. However, such biosensors are difficult to fabricate on a large scale and suffer from the lack of combined optimization of reproducibility and sensitivity in complex physiological fluids. In this work, field-effect transistor (FET) biosensors based on highly uniform semiconducting carbon nanotube (CNT) thin films are mass produced to achieve highly sensitive and selective detection of the AD core blood biomarkers of β-amyloid (Aβ). The combination of the mass-produced CNT FET sensors and oligonucleotide aptamers as efficient bioreceptors enables reliable and reproducible sub-femtomolar detection in full human serum for Aβ_{42} and Aβ_{40} peptides and has outperformed other methods reported to date. The adsorption of biological substrates to the sensor was significantly reduced by multiple blocking steps, resulting in selectivity ratios of up to 730% (Aβ_{40}) and 800% (Aβ_{42}). The aptamer-functionalized CNT FET biosensor exhibits a large dynamic range (>10^4), rapid response time (several minutes), and low variation (<10%) and can be delivered as a low-cost and rapid clinical detection technology for the early diagnosis and mass screening of AD. This platform will help bring complex laboratory-based and expensive diagnostic tools to the point of care.

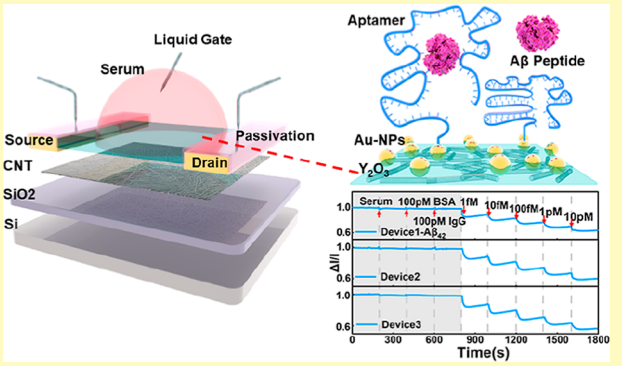

KEYWORDS: *carbon nanotube, field-effect transistor biosensor, Alzheimer's disease, Serum biomarker, Early diagnosis*

INTRODUCTION

Alzheimer's disease (AD), characterized by progressive cognitive decline, is the most common cause of dementia and affects millions of individuals aged over 65 worldwide.[1,2] Clinical pathological evidence suggests that the pathology begins 10−15 years before cognitive symptoms emerge.[3,4] Since AD progression is irreversible and incurable after the onset of cognitive symptoms, early diagnosis and intervention with disease-modifying treatments at the asymptomatic stage are crucial for the treatment of AD.[5,6] Rapid screening tests that can be widely and inexpensively deployed to identify those who might benefit from early disease-modifying treatments are urgently needed.[7,8] Current approved diagnosis methods in the clinic for AD—measurement of Aβ protein level in cerebrospinal fluid (CSF) combined with Aβ positron emission tomography (PET) imaging—are not widely applied for the screening test due to the invasiveness of lumbar punctures for obtaining CSF and high costs of PET imaging.[9−11] Diagnosed methods based on AD blood biomarkers are preferred because the collection of peripheral blood is simple, minimally invasive, and cost effective.[12,13] However, obstacles to detection still remain, such as the extremely low concentration of AD-related proteins in blood, the large dynamic range of proteins, and masking effects caused by significant levels of various interferants in blood.[14,15]

Conventional enzyme-linked immunosorbent assay (ELISA)-based techniques to assess plasma AD biomarker levels in patients have proven unsuccessful due to their insufficient sensitivity.[16,17] Although remarkable progress has been made in the ultrasensitive detection of plasma Aβ levels by using new antibody-based technologies, such as single-molecule arrays (Simoa) and immunoprecipitation mass spectrometry (IP−MS), they are too bulky, expensive, and time consuming for screening test requirements.[18,19] Advances in nanomaterial-based FETs illustrate the importance and

Received: May 3, 2022
Accepted: June 28, 2022
Published: July 11, 2022

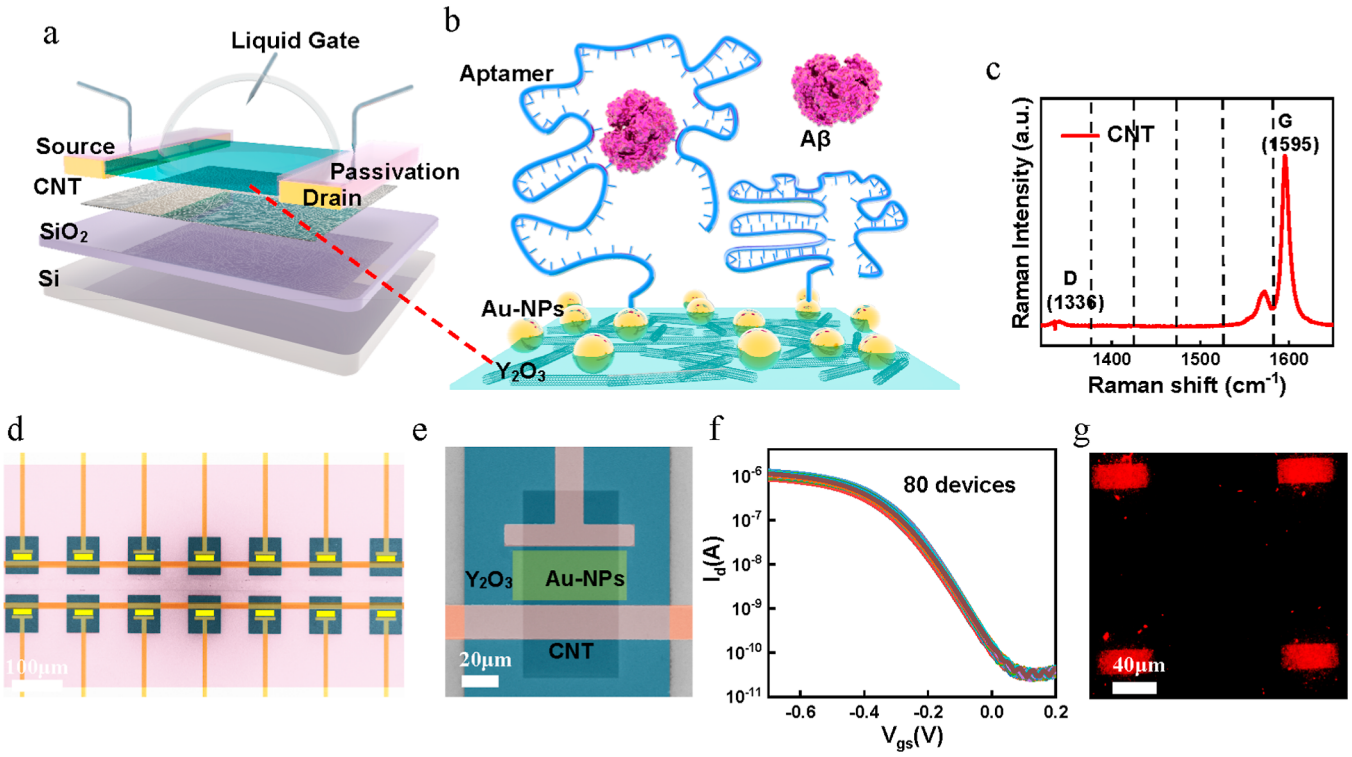

Figure 1. Fabrication and characterization of the CNT FET biosensor. (a) Schematic diagram of an aptamer-functionalized CNT FET biosensor for the detection of AD serum biomarkers. (b) Illustration of aptamer probe immobilization onto FG using a typical Au linker, followed by hybridization with Aβ peptides. (c) Raman image of sorted CNTs. (d) Scanning electron microscopy (SEM) image of the CNT FET biosensor array. The scale bar is 100 μm. (e) SEM image of the core reactive region of a biosensor. The scale bar is 20 μm. (f) Transfer curves of 80 CNT FETs (using a liquid gate) after the deposition of Au nanoparticles, V_{ds} = −0.1 V. (g) Fluorescence image of a Cy5-labeled Aβ_{42} aptamer hybridized to Au-NPs immobilized on a CNT FG FET channel surface.

promise of next-generation label-free, high-sensitivity, and high-integration biosensing techniques.[20−22] Although nano-FET biosensors outperform current bioanalytical tools in terms of sensor performance, their application in the clinical detection of blood-based biomarkers is still challenging. First, the lack of cost-effective mass production for high-performance nano-FET platforms hampers the development pace of this novel biosensing technology. The wafer-scale preparation of FETs with high uniformity in an industry-compatible way is not accessible for most nanomaterial-based FET sensors.[23−25] Second, the affinity of antibody-based receptors is always influenced by the physiological environment, such as pH, temperature, and ionic strength.[26−29] Moreover, because they are functionalized with a large receptor-like antibody (except for those using antibody fragments), the sensitivity of nano-FET sensors is fundamentally limited by the shielding effect created by the electrical double layer, which is smaller than 1 nm in typical physiological fluids.[30−32] Semiconducting CNT network films have been demonstrated to be promising channel materials for the construction of ultrasensitive and batch-fabricated FET biosensors.[33,34] Nonetheless, CNT FET-based biosensors fabricated on large scales for ultralow-concentration biomarker detection with rapid response in complex physiological environments have not yet been demonstrated.

In this work, nucleic acid aptamer-functionalized CNT FETs are manufactured using a high-throughput fabrication process to construct a highly sensitive and selective biosensor array for the detection of low-concentration Aβ proteins in serum and to promote FET-based sensor clinical applications in the early diagnosis of AD. The sensor array exploits a highly uniform semiconducting CNT network film as an ultrathin active channel and DNA aptamers modified on a floating gate (FG) insulator as selective receptors for Aβ_{40} and Aβ_{42} peptides. The aptamer-functionalized CNT FETs can repeatedly detect Aβ_{40} and Aβ_{42} peptides in both 1× PBS and undiluted serum with a limit of detection (LoD) as low as 50 aM. These sensors also exhibit high selectivity with the response ratio to the target Aβ peptides and nontarget masking proteins such as human IgG and albumin (defined as selectivity ratio) of up to 800%, outperforming all the other AD biomarker sensing methods. The CNT FET biosensors also demonstrate a large dynamic range, high accuracy, and low variation with the characteristics of over four decades of linear analytical range, a high recovery range of 88−108%, and sensor-to-sensor variation of less than 10%. Moreover, with such robust and sensitive sensors, we can achieve real-time detection of these AD serum biomarkers in a few minutes. These results indicate the great potential of aptamer-functionalized CNT FET biosensors in early diagnosis and mass screening tests for AD.

RESULTS AND DISCUSSION

Fabrication and Characterization of CNT FET Biosensors. A structural schematic illustration of the aptamer-functionalized CNT FET biosensor used in this work is shown in Figure 1a. The device is constructed with a semiconducting CNT network film as the active channel, a Y_2O_3 film as the gate dielectric, and Au particles as the linkers for connecting the probes (DNA aptamers in this work, as shown in Figure 1b). CNT films with high semiconducting purity (>99.99%)

https://doi.org/10.1021/acssensors.2c00967
ACS Sens. 2022, 7, 2075−2083

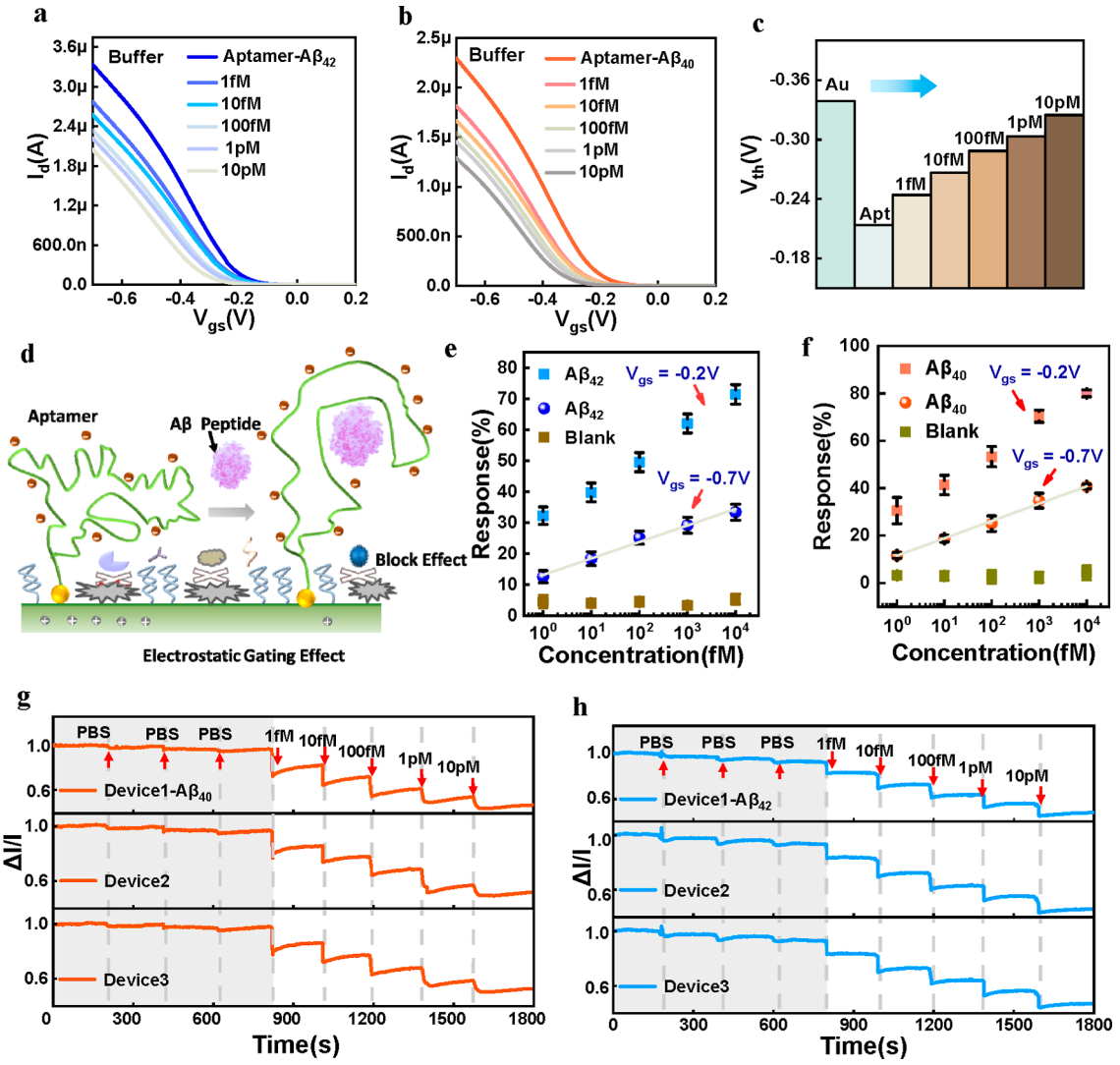

Figure 2. AD core biomarker detection by aptamer-functionalized CNT FET sensors in PBS. (a) Transfer curve evolution of the CNT FET biosensor measured after the introduction of various Aβ_{42} and (b) Aβ_{40} concentrations ranging from 1 fM to 10 pM. (c) Threshold voltage changes of CNT FET after each step of functionalization chemistry and again after exposure to different target concentrations for the detection of Aβ_{40}. (d) Diagram of structure changes of the aptamer before and after capture of the target protein and the blocking effect of the sensor in solution. (e,f) Calibration curves of the CNT FET biosensor at V_{gs} = −0.7 V and V_{gs} = −0.2 V under a low and fixed V_{ds} = −0.1 V for different concentrations of the AD biomarker peptides (e) Aβ_{42} and (f) Aβ_{40}. The black dashed line represents the blank control immersed in 1× PBS solution (dark yellow). The error bars in e and f indicate the standard deviation calculated from the 10 sensors. (g) Real-time record of current I_{ds} changes for three different devices after the sequential addition of PBS and different concentrations of Aβ_{42} and (h) Aβ_{40} peptides at V_{gs} = −0.2 V and V_{ds} = −0.1 V.

were deposited onto 4 in. Si/SiO_2 substrates by a solution-derived method.[34] We characterized the CNT films by Raman spectroscopy, as shown in Figure 1c. The intensity ratio of the G-peak to the D-peak of the Raman spectrum is 10:1, indicating that the CNTs have few defects. As illustrated in the Methods and Figure S1, the fabrication process of CNT FET biosensors is compatible with the conventional micro-fabrication process, which enables the mass production of sensor devices needed for low-cost AD screening. The fabricated sensor array (Figure 1d) consists of 22 devices with a channel length/width of 20 μm/40 μm. We covered the entire CNT film with a 6 nm ultrathin Y_2O_3 film as a dielectric layer (3 nm Y metal film oxidized for 30 min) and then deposited 0.6 nm Au-NPs by electron beam evaporation onto the Y_2O_3 surface. All the metal contacts and electrodes of the sensors were encapsulated with a photoresist layer to prevent any leakage current and electrochemical reaction in the liquid environment, and a window with a length of 17 mm and a width of 40 mm was opened for each biosensor to enable liquid gate testing (see the SEM of a typical fabricated sensor in Figure 1e). We randomly measured the transfer curves of 80 FETs on a 4 in. wafer with 1× PBS (Figure 1f). All transistors exhibit p-FET properties with a current on/off ratio of approximately 10^5, demonstrating the high semiconducting purity of the sorted CNTs. The output curve (Figure S2b) of the FET exhibits good linearity, indicating that stable ohmic contacts are formed between Pd and CNTs. The almost hysteresis-free and low subthreshold slope (SS) transfer curves demonstrate that the CNT FET has few defects and can reliably reflect the charge change on the FG (Figure S2a). Statistical analysis shows a highly uniform distribution of threshold voltage with very small standard deviations of only 8 mV (Figure S2c). The on-state current at V_{gs} = −0.7 V of the 80 devices is distributed between 0.8 and 1.3 μA with an

https://doi.org/10.1021/acssensors.2c00967
ACS Sens. 2022, 7, 2075−2083

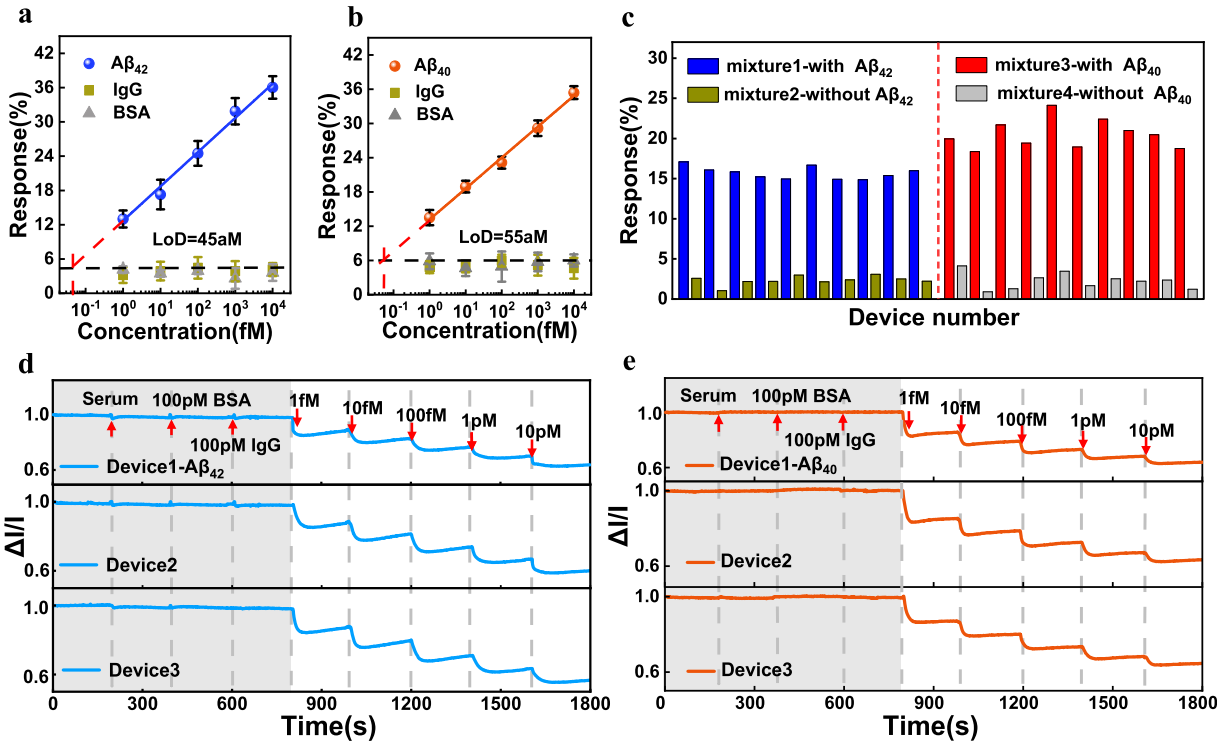

Figure 3. Sensitivity and selectivity of aptamer-functionalized CNT FET sensors in serum. (a,b) Calibration curve of the sensor array for the detection of Aβ_{42} and Aβ_{40} in serum. There is almost no response to human IgG and BSA at a similar concentration to the target. The error bars in (a,b) indicate the standard deviation calculated from the 10 sensors. LoD is defined as the concentration showing a response equal to $Y = Y_C + kS_c$, where Y_C is the mean value of the response of the control group, S_c is the standard deviation, and k is selected as 3 here. (c) Aβ_{42} in mixture 1 and mixture 2 and Aβ_{40} peptide in mixture 3 and mixture 4 were used to test aptamer-functionalized CNT FET sensors. All tests were performed by adding 20 μL of the mixture to the sensor after incubation for 30 min. (d,e) Real-time responses of three CNT FET biosensors upon sequentially adding different concentrations of solutions, including serum, BSA, IgG, and targets from 1 fM to 10 pM at V_{gs} = −0.2 V and V_{ds} = −0.1 V.

average of approximately 1.023 μA (Figure S2d) and a standard deviation of 0.088 μA. All these statistical results demonstrated reproducible underlying devices for constructing reliable biosensors. To construct CNT FG FET sensors for AD biomarkers, specific thiolated DNA aptamers were immobilized onto the sensor channels with the as-deposited Au-NPs for linking. Aptamers are used in biosensors as high-affinity bioreceptors that are much less expensive and more robust than antibodies.[35,36] Figure 1g shows a fluorescent image of four unpassivated CNT FET sensor devices after incubation with 3′ terminal Cy5-labeled and 5′ terminal thiolated DNA aptamers. [37]After thorough washing, we can see that the fluorescence comes only from channel areas covered with Au nanoparticles in Figure 1g (red), while there is no fluorescence outside the channels (dark), indicating the successful selective modification of aptamers onto the Au-NPs FG with Au−S bonds.

AD Core Biomarker Detection in PBS. After successful functionalization, we first investigated the sensing behaviors of Aβ aptamer-functionalized CNT FET sensors in PBS. Amyloid-β (Aβ_{42} and Aβ_{40}) peptides are deposited in the CSF to form neuroinflammatory plaques that trigger pathogenic cascade reactions to cause AD-related symptoms.[38,39] The detection of Aβ peptide concentrations can be effective in preventing AD and aiding positive recovery from treatment. In contrast to previous studies on antibody biosensors, the aptamers for AD core biomarkers of Aβ_{40} and Aβ_{42} peptides were the first application in FET-type biosensors. The detailed sequence information is shown in Table S1 and Figure S3. Two kinds of aptamer-functionalized CNT FET sensors and their response to Aβ_{40} and Aβ_{42} were then investigated in 1× PBS. The 1× PBS solution reproduces a simulated physiologically relevant environment with a pH of 7.4 and an ionic strength of 162 mM (both similar to those in blood serum). The CNT FETs show a positive shift in the threshold voltage after aptamer functionalization (Figure S4), which means that the negatively charged backbones are fixed to the Au-NPs decorated on the Y_2O_3 insulator. Typical transfer curves before and after the addition of Aβ_{40} and Aβ_{42} peptides with concentrations ranging over 5 orders of magnitude were measured and are shown in Figure 2a,b. The threshold voltage of the transfer curves shifts to the left (Figures 2c and S5), and the on-state current decreases as the target concentration increases from 1 fM to 10 pM. Upon hybridization with the corresponding targets, the secondary structures of these aptamers undergo conformational change from a folded state to a stretched state,[40] which moves the negative charge distribution region of the aptamer away from the CNT channel, leading to a reduction in the current (Figure 2d). Figure S6 shows the energy band changes of the CNT devices before and after capturing the targets. A sensor without aptamer functionalization was measured under the same conditions and taken as a blank control group (Figure S7). The static sensor response here is defined as the relative change in the drain current at certain gate voltages (response = $|I_{ds} - I_{ds0}|/I_{ds0}$, where I_{ds0} and I_{ds} are the drain current before and after target incubation). The responses of sensors to different Aβ_{40} and Aβ_{42} peptide concentrations in the linear

https://doi.org/10.1021/acssensors.2c00967
ACS Sens. 2022, 7, 2075−2083

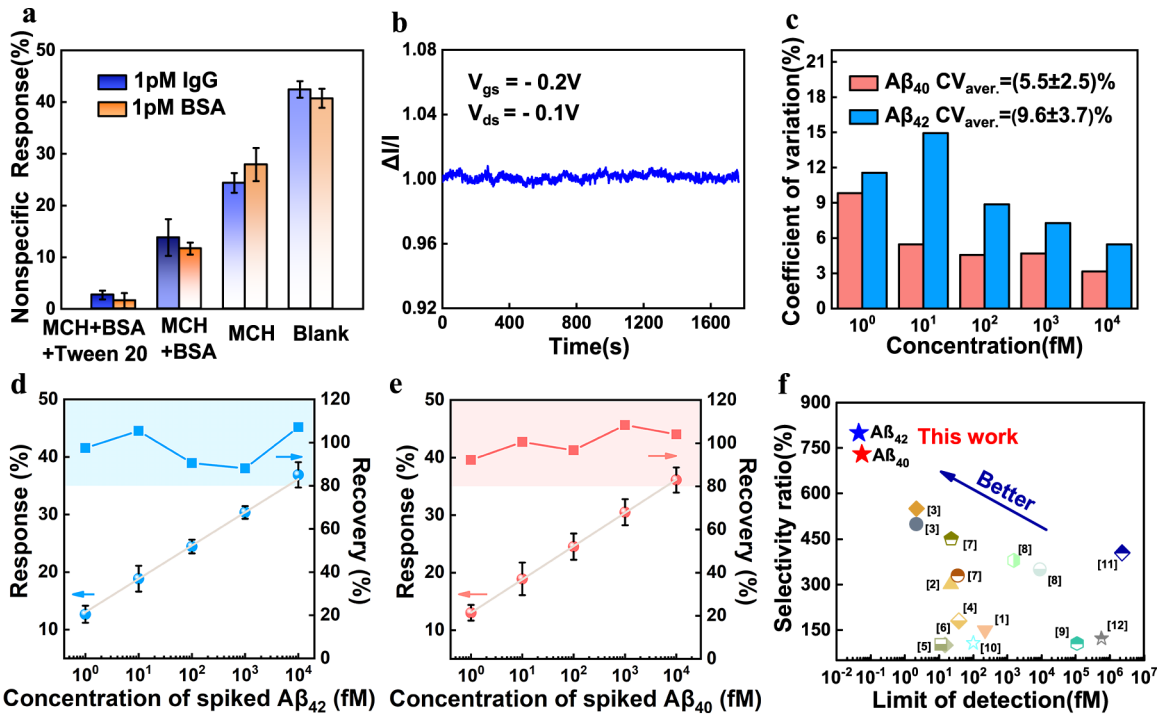

Figure 4. Performance evaluation and benchmarking of the CNT FET biosensor. (a) Blocking effect of different blocking agents on biosensors. (b) Stability measurement of a typical CNT FET in serum under V_{gs} = −0.2 V and V_{ds} = −0.1 V. (c) Coefficient of variation of the response from 10 sensors in each group at different target protein concentrations for the detection of Aβ_{42} peptide and Aβ_{40} peptide in serum. The coefficient of variation was defined as CV = (SD/average) × 100%, where SD is the standard deviation of the concentration and average is the average of the 10 devices. (d,e) Recovery of Aβ_{42} and Aβ_{40} peptides in human serum. (f) Performance benchmark comparing different detection platforms and other sensors reported in the literature (for reference number, see Table S3). The ratio of the response values to the target Aβ peptides and nontarget proteins in Figure 3c is defined as the selectivity ratio.

regime (V_{gs} = −0.7 V) and subthreshold regime (V_{gs} = −0.2 V) are plotted in Figures 2e,f, respectively. An obvious linear relationship (with R^2 > 0.99) between the current change of the sensor and the logarithmic concentration of the biomarkers was observed at −0.7 V in the range of 10^0−10^4 fM. As a comparison, the sensor exhibits a higher sensitivity but a worse linearity in the subthreshold regime than in the linear regime. The subthreshold operation offers larger responses due to a steep subthreshold swing (see Figure S10b), and an exponential change in the drain current is expected when the gate voltage changes linearly, which is consistent with a previous report. The high selectivity is proven by the response of less than 6% in the blank control group compared with that of up to 40−90% in the experimental groups. In addition to the static test, we performed a study of the real-time detection capability of the CNT FET biosensors in PBS buffer for the Aβ_{42} peptide and Aβ_{40} peptide (Figure 2g,h). The time-dependent change in the current I_{ds} was recorded, and the arrows indicate the moment the sample solutions were added. Sample solutions with different analytes and a concentration of 2 μL were dropped onto the biosensors every 200 s. The current was almost unchanged after three washes with PBS buffer. Then, the current decreases from the baseline value upon subsequent addition of sample solutions with increasing concentrations of Aβ_{42} peptide and Aβ_{40} peptides (from 1 fM to 10 pM) in 1× PBS buffer. These results in PBS demonstrated that the fixed aptamer receptors can capture the peptide targets stably and sense conformational changes in high ionic strength solutions sensitively, which lays the foundation for sensitive detection in serum.

Sensitivity and Selectivity of Aptamer-Functionalized CNT FET Sensors in Serum. We then evaluated the sensitivity and selectivity of aptamer-functionalized CNT FET sensors in human serum. Healthy human blood samples were purchased from Beijing Laboratory Biotechnology Co., Ltd. Most of the blood cells were removed by low-speed centrifugation, and the upper liquid layer was taken as serum. To demonstrate the detection capability in serum, Aβ peptides were spiked into the serum to obtain different concentrations of Aβ peptides from 1 fM to 10 pM, which covers the physiological range of Aβ in both blood and CSF. After the corresponding aptamer modification, a multi-blocking process (see Methods) was followed to avoid any nonspecific proteins on the FET surface. The transfer curves were measured after the aptamer-functionalized FET sensors were incubated with serum solution with different Aβ peptide concentrations and then provided fundamental data to characterize the sensors. We determined the selectivity of the aptamer-functionalized CNT FET biosensor to nontarget proteins by measuring the sensor response to other proteins, such as BSA and human IgG, at various concentrations (Figure 3a,b). BSA was used to mimic the additional effect of human serum albumins. The sensor exhibits a positive shift in transfer curves (see Figure S8) and a high response to drain current as the concentration increases (Figure 3a,b), similar to the behaviors measured in PBS, and the high sensitivity of the aptamer-functionalized CNT FET enables the detection of targets in a complex serum environment. The sensor shows high sensitivity to moderate changes in target concentration even with a detection range of 5 orders of magnitude (Figure 3a,b), while it exhibits a

https://doi.org/10.1021/acssensors.2c00967
ACS Sens. 2022, 7, 2075−2083

negligible response to interferents (PBS or IgG) in the whole dynamic range. The limit of detection (LoD), which was customarily computed as the concentration providing a response equal to the average noise level (taken from the control groups of human IgG here) plus three times the noise standard deviation, was calculated to be 55 and 45 aM for $A\beta_{40}$ and $A\beta_{42}$ in serum, respectively. To further investigate the specificity of the sensor to distinguish between $A\beta_{40}$ and $A\beta_{42}$ in complex solutions, 10 other sensors modified with $A\beta_{42}$ aptamer ($A\beta_{40}$ aptamer) were used to detect the response to the mixture of serum solution with and without 10 fM $A\beta_{42}$ ($A\beta_{40}$) peptides. The mixed solutions were prepared with the addition of 1 nM BSA, 1 nM IgG, and 1 nM $A\beta_{40}$ ($A\beta_{42}$) peptides into the full serum. As shown in Figure 3c, for Mix1 (with $A\beta_{42}$) and Mix3 (with $A\beta_{40}$) containing the corresponding targets, all 10 sensors responded above 15%, three times larger than the response value of 5% to Mix2 (without $A\beta_{42}$) and Mix4 (without $A\beta_{40}$). To evaluate the sensing capability in fast blood-based screening tests, we show real-time sensor measurements while going through changing serum solutions with spiked $A\beta$ concentrations ranging from 1 fM to 1 pM. In these measurements, CNT FET sensors were operated in maximum sensitivity mode with similar operation in PBS, that is, applying V_{gs} corresponding to the subthreshold regime at a given bias (V_{gs} = −0.2 V, V_{ds} = −0.1 V). As shown in Figure 3d,e, the aptamer-functionalized CNT FET sensor identified the spiked $A\beta$ peptide concentration down to 1 fM with a response time of approximately 40 s, while the influence of serum, BSA, and IgG was negligible. These results indicate that the aptamer-functionalized CNT FET sensor has excellent selectivity and sensitivity for the analysis of AD biomarkers in real biological samples.

Performance Evaluation and Benchmarking of the CNT FET Biosensor. To further evaluate the sensing performance of our biosensors in serum, we conducted detailed investigations on the blocking effect, variation, stability, and recovery tests. The multi-blocking process was performed in human serum, and the nonspecific responses were compared to those obtained with different blocking processes. As shown in Figure 4a, the biosensor response to nontargets was reduced from 50 to <5% by using a three-step blocking with MCH, Tween 20, and BSA. It effectively reduces the adsorption of molecules from serum onto the sensor and improves the sensitivity of serum biomarker detection. We further recorded the current variation of the CNT FET biosensor with time to evaluate its stability performance in serum at V_{gs} = −0.7 V and V_{ds} = −0.1 V. Bias stress measurements of the CNT FET biosensor showed stability in serum for more than 30 min (Figure 4b), suggesting that the dense Y_2O_3 film effectively isolates the CNT film from the biological matrix and enables the sensor to function properly under prolonged liquid conditions. Excellent reliability, including performance stability and uniformity, is critical for the applications of sensors in point-of-care testing (POCT). The coefficient of variation (CV) is used here as an important evaluation index of sensor reliability to reflect the response variation across devices at the same target concentration. The responses to the targets in Figure 3a,b are based on a group of 10 devices from 1 fM to 10 pM and calculate the CV within 10% (Figure 4c). We performed the recovery test with average recoveries of 88−108% in the linear working range (Figure 4d,e and Table S2), which indicates that the CNT FET biosensor can be employed for a precise evaluation of $A\beta_{42}$ and $A\beta_{40}$ peptides in serum samples. Performance benchmarking between different detection platforms reported in the literature is presented in Figure 4f. Compared with the reported conductance, photocurrent, surface plasma resonance, voltammetry, colorimetric and impedance methods (for detailed references, see Supporting Information Table S3), the aptamer-functionalized CNT FETs provided the best performance for the detection of $A\beta_{40}$ peptide and $A\beta_{42}$ in terms of LoD and selectivity ratio. The ultralow LoDs of 55 aM (red star) for $A\beta_{40}$ and 45 aM (blue star) for $A\beta_{42}$ are the lowest concentrations detected in serum to date. As another important parameter for biosensors, selectivity is a very large challenge, especially when the sensor is in a complex serum or in a clinical sample. In this paper, ultrahigh selectivity ratios of 730% and 800% were achieved for $A\beta_{40}$ peptide and $A\beta_{42}$ peptide in serum, respectively, and are simultaneously higher than the best reported results for sensors built based on aligned CNT arrays.[20] Moreover, our platform based on network CNT thin films can offer wafer-scale uniformity and a feasible fabrication process, which is not available for other nanomaterial films to date. All of these advantages suggest that our aptamer-functionalized CNT FET biosensors have potential in the early diagnosis of AD patients in community screening with a rapid and minimally invasive technique.

CONCLUSIONS

In summary, we fabricated wafer-scale aptamer-functionalized FET biosensors based on randomly oriented semiconducting CNT network films and explored the sensing performance to detect Alzheimer's disease serum biomarkers in 1× PBS and undiluted human serum. The aptamer-functionalized CNT FETs demonstrated a wide analytical range with ultralow LoDs to 45 aM for $A\beta_{42}$ and 55 aM for $A\beta_{40}$. The multi-blocking step on the sensor effectively reduces nonspecific adsorption from the biological matrix and efficiently improves the selectivity ratio by up to 800%, even in mixed solutions with structurally similar proteins. In addition, the biosensors showed high accuracy with a recovery rate of approximately 88−108%, long-term stability in serum, and high uniformity with device-to-device variation of less than 10% (10 devices). Based on these excellent sensing properties and reliability, aptamer-functionalized CNT FET biosensors have great potential as reliable low-cost fast clinical sensing platforms and will constitute a great advance in early diagnosis and mass screening tests for AD.

EXPERIMENTAL METHODS

Materials. Raw arc-discharged SWNTs were obtained from Carbon Solution Inc. The dispersants (poly[9-(1-octylonyl)-9*H*-carbazole-2,7-diyl](PCz)) were synthesized by Suzuki polycondensation. The previously reported aptamers for $A\beta_{42}$ and $A\beta_{40}$ peptides were purchased from Sangon Biotech Co., Ltd. (Shanghai, China), and the sequences of DNA aptamers used in this paper are listed in Table S1.[37,41] Healthy human blood samples were purchased from Beijing Laboratory Biotechnology Co., Ltd. Most blood cells were removed by low-speed centrifugation, and the upper liquid layer was taken as serum. $A\beta$ peptide powders were purchased from Beijing Feimer Biotechnology Co. These powders were dissolved in 1× PBS solution or serum solution for dilution before electrical measurements. The concentration was calculated as equivalent concentrations to the $A\beta$ monomer. 6-Mercapto-1-hexanol (MCH) was purchased from J&K Scientific. Chemicals such as tris(2-carboxyethyl)phosphine hydrochloride (TCEP), Tween 20 (500 mL), bovine serum albumin (BSA, 98%), and immunoglobulin G (IgG, 95%) were purchased

https://doi.org/10.1021/acssensors.2c00967
ACS Sens. 2022, 7, 2075−2083

from Sigma-Aldrich. Phosphate buffer solution (PBS) with a pH of 7.4 was purchased from Sangon Biotech.

Fabrication of CNT FG FET Biosensors. Polymer-sorted solution-derived semiconducting CNTs were deposited onto 4 in. Si/SiO_2 substrates. First, aptamer-functionalized CNT-based FG-FET 0.3/20/40 nm Ti/Pd/Au stacked metal films were deposited by electron beam evaporation to form a source and drain. Then, the channel region was patterned by UV lithography, followed by reactive ion etching (RIE). Ti/Au stacked films with dimensions of 20/60 nm were deposited as pads. Then, Y with a thickness of 3 nm was formed by electron beam evaporation, and dense Y_2O_3 films (Figure S9) were oxidized at 270° for 30 min to form oxide dielectrics. Stacked films of Au (0.6 nm) were deposited in the center of the channel. Finally, after S1813 photoresist passivation, a window was opened in the device channel to facilitate electrical testing (Figure S1). The electrical properties of the devices were examined using a parameter analyzer (Keithley 4200A-SCS).

Functionalization and Characterization of Aptamer on CNT FG FET Biosensors. The aptamers were diluted with 1× PBS, and the S−S bond was opened using tris(2-carboxyethyl)phosphine hydrochloride (TCEP, from Sigma-Aldrich) as a reducing agent. Then, 20 μL of the mixture of 10 μM aptamer and 10 mM TCEP was reacted overnight in the biosensor trench region. The aptamer can form a stable Au−S structure by hybridization with gold particles. All biosensors were designed to provide sufficient site-immobilized aptamers to improve the response. After incubation, the device was thoroughly washed with 1× PBS to remove the unreacted ligands and then gently blown dry with nitrogen gas. To block nonspecific adsorption, 2 mM 6-mercapto-1-hexanol (MCH, from J&K Scientific) was utilized as a blocking agent for 0.5 h, followed by incubation with a mass score of 0.5% Tween 20 and 1 mM BSA for 1.5 h. To determine whether the inducer can be successfully modified on the FET sensor surface, the Cy5-labeled aptamer was modified with a sulfhydryl group at the other end after an equal volume mixture of 10 μM aptamer and 10 mM TCEP of the aptamer was incubated on the photoresist-free sensor surface. After a full night, the sensor surface was repeatedly washed with pure water, and the chip was then observed under a fluorescence microscope.

■ ASSOCIATED CONTENT

Supporting Information

The Supporting Information is available free of charge at https://pubs.acs.org/doi/10.1021/acssensors.2c00967.

Schematic diagram of the microfabrication process of CNT FG FET biosensors, SEM images of Y_2O_3 and Au particles, electrical performance of CNT FET, evolution of the transfer curve from the original device (Au) to the aptamer-modified (probe) biosensor to the target concentration, electrical performance of the sensor in serum, recovery tests, energy band changes, and detailed information on aptamer sequences and sensing performance comparison (PDF)

■ AUTHOR INFORMATION

Corresponding Authors

Mengmeng Xiao − *Key Laboratory for the Physics and Chemistry of Nanodevices and Center for Carbon-based Electronics, School of Electronics, Peking University, Beijing 100871, China; Jihua Laboratory, Foshan 528200, China*; Email: mmxiao@pku.edu.cn

Zhiyong Zhang − *Hunan Institute of Advanced Sensing and Information Technology, Xiangtan University, Xiangtan 411105, China; Key Laboratory for the Physics and Chemistry of Nanodevices and Center for Carbon-based Electronics, School of Electronics, Peking University, Beijing 100871, China; Jihua Laboratory, Foshan 528200, China*; orcid.org/0000-0003-1622-3447; Email: zyzhang@pku.edu.cn

Authors

Hong Chen − *Hunan Institute of Advanced Sensing and Information Technology, Xiangtan University, Xiangtan 411105, China*

Jianping He − *Hunan Institute of Advanced Sensing and Information Technology, Xiangtan University, Xiangtan 411105, China*

Yang Zhang − *Hunan Institute of Advanced Sensing and Information Technology, Xiangtan University, Xiangtan 411105, China*

Yuqi Liang − *Key Laboratory for the Physics and Chemistry of Nanodevices and Center for Carbon-based Electronics, School of Electronics, Peking University, Beijing 100871, China*

Haiyang Liu − *Key Laboratory for the Physics and Chemistry of Nanodevices and Center for Carbon-based Electronics, School of Electronics, Peking University, Beijing 100871, China*

Complete contact information is available at: https://pubs.acs.org/10.1021/acssensors.2c00967

Author Contributions

‖H.C. and M.X. contributed equally to this work.

Notes

The authors declare no competing financial interest.

■ ACKNOWLEDGMENTS

This work was supported by the National Natural Science Foundation of China (grant no. 62174007 and U21A6004), the Beijing Municipal Science and Technology Commission (grant no. Z191100007019001-3), the Basic and Applied Basic Research Major Programme of Guangdong Province, China (grant no. 2021B0301030003), and Jihua Laboratory (project no. X210141TL210).

■ REFERENCES

(1) Lennart, M. Alzheimer's disease. *Nature* **2009**, *461*, 895−897.

(2) Alzheimer's Association. 2008 Alzheimer's disease facts and figures. *Alzheimer's Dementia* **2008**, *4*, 110−133.

(3) Lleó, A.; Cavedo, E.; Parnetti, L.; Vanderstichele, H.; Herukka, S. K.; Andreasen, N.; Ghidoni, R.; Lewczuk, P.; Jeromin, A.; Winblad, B.; Tsolaki, M.; Mroczko, B.; Visser, P. J.; Santana, I.; Svenningsson, P.; Blennow, K.; Aarsland, D.; Molinuevo, J. L.; Zetterberg, H.; Mollenhauer, B. Cerebrospinal fluid biomarkers in trials for Alzheimer and Parkinson diseases. *Nat. Rev. Neurol.* **2015**, *11*, 41−55.

(4) Jansen, W. J.; Ossenkoppele, R.; Tijms, B. M.; Fagan, A. M.; Hansson, O.; Klunk, W. E.; Vander, W. M.; Villemagne, V. L.; Frisoni, G. B.; Fleisher, A. S.; Lleó, A.; Mintun, M. A.; Wallin, A.; Engelborghs, S.; Na, D. L.; Chételat, G.; Molinuevo, J. L.; Landau, S. M.; Mattsson, N.; Kornhuber, J.; Sabri, O.; Rowe, C. C.; Parnetti, L.; Popp, J.; Fladby, T.; Jagust, W. J.; Aalten, P.; Lee, D. Y.; Vandenberghe, R.; Resende de Oliveira, C.; Kapaki, E.; Froelich, L.; Ivanoiu, A.; Tomasz, G.; Verbeek, M. M.; Sanchez, J. P.; Hildebrandt, H.; Camus, V.; Zboch, M.; Brooks, D. J.; Drzezga, A.; Rinne, J. O.; Newberg, A.; de Mendonça, A.; Sarazin, M.; Rabinovici, G. D.; Madsen, K.; Kramberger, M. G.; Nordberg, A.; Mok, V.; Mroczko, B.; Wolk, D. A.; Meyer, P. T.; Tsolaki, M.; Scheltens, P.; Verhey, F. R. J.; Visser, P. J. Association of Cerebral Amyloid-β Aggregation With Cognitive Functioning in Persons Without Dementia. *JAMA Psychiatr.* **2018**, *75*, 84.

(5) Burgener, S. C.; Dickerson-Putman, J. ASSESSING PATIENTS in the Early Stages of Irreversible Dementia. The relevance of patient perspectives. *J. Gerontol. Nurs.* **1999**, *25*, 33−41.

(6) Rasmussen, J.; Langerman, H. Alzheimer's Disease - Why We Need Early Diagnosis. *Degener. Neurol. Neuromuscul. Dis.* **2019**, *9*, 123−130.
(7) Janelidze, S.; Mattsson, N.; Palmqvist, S.; Smith, R.; Beach, T. G.; Serrano, G. E.; Chai, X.; Proctor, N. K.; Eichenlaub, U.; Zetterberg, H.; Blennow, K.; Reiman, E. M.; Stomrud, E.; Dage, J. L.; Hansson, O. Plasma P-tau181 in Alzheimer's disease: relationship to other biomarkers, differential diagnosis, neuropathology and longitudinal progression to Alzheimer's dementia. *Nat. Med.* **2020**, *26*, 379.
(8) Thijssen, E. H.; La, R.; La Joie, R.; Wolf, A.; Strom, A.; Wang, P.; Iaccarino, L.; Bourakova, V.; Cobigo, Y.; Heuer, H.; Spina, S.; VandeVrede, L.; Chai, X.; Proctor, N. K.; Airey, D. C.; Shcherbinin, S.; Duggan Evans, C.; Sims, J. R.; Zetterberg, H.; Blennow, K.; Karydas, A. M.; Teunissen, C. E.; Kramer, J. H.; Grinberg, L. T.; Seeley, W. W.; Rosen, H.; Boeve, B. F.; Miller, B. L.; Rabinovici, G. D.; Dage, J. L.; Rojas, J. C.; Boxer, A. L.; Knopman, D. S.; Graff-Radford, N.; Grossman, M.; Huey, E. H.; Onyike, C.; Kaufer, D.; Roberson, E.; Ghoshal, N.; Weintraub, S.; Appleby, B.; Litvan, I.; Kerwin, D.; Mendez, M.; Bordelon, Y.; Coppola, G.; Ramos, E. M.; Tartaglia, M. C.; Hsiung, G. Y.; MacKenzie, I.; Domoto-Reilly, K.; Foroud, T.; Dickerson, B. C. Treatment for frontotemporal lobar degeneration, diagnostic value of plasma phosphorylated tau181 in Alzheimer's disease and frontotemporal lobar degeneration. *Nat. Med.* **2020**, *26*, 387−397.
(9) Gupta, V.; Sundaram, R.; Martins, R. N. Multiplex biomarkers in blood. *Alzheimer's Res. Ther.* **2013**, *5*, 31.
(10) Fortea, J.; Carmona-Iragui, M.; Benejam, B.; Fernández, S.; Videla, L.; Barroeta, I.; Alcolea, D.; Pegueroles, J.; Muñoz, L.; Belbin, O.; de Leon, M. J.; Maceski, A. M.; Hirtz, C.; Clarimón, J.; Videla, S.; Delaby, C.; Lehmann, S.; Blesa, R.; Lleó, A. Plasma and CSF biomarkers for the diagnosis of Alzheimer's disease in adults with Down syndrome: a cross-sectional study. *Lancet Neurol.* **2018**, *17*, 860−869.
(11) Chen, Q.; Du, Y.; Zhang, K.; Liang, Z.; Li, J.; Yu, H.; Ren, R.; Feng, J.; Jin, Z.; Li, F.; Sun, J.; Zhou, M.; He, Q.; Sun, X.; Zhang, H.; Tian, M.; Ling, D. Tau-Targeted Multifunctional Nanocomposite for Combinational Therapy of Alzheimer's Disease. *ACS Nano* **2018**, *12*, 1321−1338.
(12) Nakamura, A.; Kaneko, N.; Villemagne, V. L.; Kato, T.; Doecke, J.; Doré, V.; Fowler, C.; Li, Q.-X.; Martins, R.; Rowe, C.; Tomita, T.; Matsuzaki, K.; Ishii, K.; Ishii, K.; Arahata, Y.; Iwamoto, S.; Ito, K.; Tanaka, K.; Masters, C. L.; Yanagisawa, K. High performance plasma amyloid-β biomarkers for Alzheimer's disease. *Nature* **2018**, *554*, 249.
(13) Qu, Y.; Ma, Y.-H.; Huang, Y.-Y.; Ou, Y.-N.; Shen, X.-N.; Chen, S.-D.; Dong, Q.; Tan, L.; Yu, J.-T. Blood biomarkers for the diagnosis of amnestic mild cognitive impairment and Alzheimer's disease: A systematic review and meta-analysis. *Neurosci. Biobehav. Rev.* **2021**, *128*, 479−486.
(14) Song, F.; Poljak, A.; Valenzuela, M.; Mayeux, R.; Smythe, G. A.; Sachdev, P. S. Meta-analysis of plasma amyloid-β levels in Alzheimer's disease. *J. Alzheimer's Dis.* **2011**, *26*, 365−375.
(15) Galasko, D.; Golde, T. E. Biomarkers for Alzheimer's disease in plasma, serum and blood - conceptual and practical problems. *Alzheimer's Res. Ther.* **2013**, *5*, 10.
(16) De Meyer, S.; Schaeverbeke, J. M.; Verberk, I. M. W.; Gille, B.; De Schaepdryver, M.; Luckett, E. S.; Gabel, S.; Bruffaerts, R.; Mauroo, K.; Thijssen, E. H.; Stoops, E.; Vanderstichele, H. M.; Teunissen, C. E.; Vandenberghe, R.; Poesen, K. Comparison of ELISA- and SIMOA-based quantification of plasma Aβ ratios for early detection of cerebral amyloidosis. *Alzheimer's Res. Ther.* **2020**, *12*, 162.
(17) Oh, E. S.; Mielke, M. M.; Rosenberg, P. B.; Jain, A.; Fedarko, N. S.; Lyketsos, C. G.; Mehta, P. D. Comparison of conventional ELISA with electrochemiluminescence technology for detection of amyloid -β in plasma. *J. Alzheimer's Dis.* **2010**, *21*, 769−773.
(18) Li, D.; Mielke, M. M. An Update on Blood-Based Markers of Alzheimer's Disease Using the SiMoA Platform. *Neurol. Ther.* **2019**, *8*, 73−82.
(19) Schindler, S. E.; Bollinger, J. G.; Ovod, V.; Mawuenyega, K. G.; Li, Y.; Gordon, B. A.; Holtzman, D. M.; Morris, J. C.; Benzinger, T. L. S.; Xiong, C.; Fagan, A. M.; Bateman, R. J. High-precision plasma β-amyloid 42/40 predicts current and future brain amyloidosis. *Neurology* **2019**, *93*, E1647−E1659.
(20) Kim, K.; Kim, M.-J.; Kim, D. W.; Kim, S. Y.; Park, S.; Park, C. B. Clinically accurate diagnosis of Alzheimer's disease via multiplexed sensing of core biomarkers in human plasma. *Nat. Commun.* **2020**, *11*, 119.
(21) Oh, J.; Yoo, G.; Chang, Y. W.; Kim, H. J.; Jose, J.; Kim, E.; Pyun, J.-C.; Yoo, K.-H. A carbon nanotube metal semiconductor field effect transistor-based biosensor for detection of amyloid-beta in human serum. *Biosens. Bioelectron.* **2013**, *50*, 345−350.
(22) Guo, K.; Wustoni, S.; Koklu, A.; Díaz-Galicia, E.; Moser, M.; Hama, A.; Alqahtani, A. A.; Ahmad, A. N.; Alhamlan, F. S.; Shuaib, M.; Pain, A.; McCulloch, I.; Arold, S. T.; Grünberg, R.; Inal, S. Rapid single-molecule detection of COVID-19 and MERS antigens via nanobody-functionalized organic electrochemical transistors. *Nat. Biomed. Eng.* **2021**, *5*, 666−677.
(23) Lee, H. W.; Kang, D.-H.; Cho, J. H.; Lee, S.; Jun, D.-H.; Park, J.-H. Highly Sensitive and Reusable Membraneless Field-Effect Transistor (FET)-Type Tungsten Diselenide (WSe_2) Biosensors. *ACS Appl. Mater. Interfaces* **2018**, *10*, 17639−17645.
(24) Shan, J.; Li, J.; Chu, X.; Xu, M.; Jin, F.; Wang, X.; Ma, L.; Fang, X.; Wei, Z.; Wang, X. High sensitivity glucose detection at extremely low concentrations using a MoS_2-based field-effect transistor. *RSC Adv.* **2018**, *8*, 7942−7948.
(25) Usman Ali, S. M.; Nur, O.; Willander, M.; Danielsson, B. Glucose Detection With a Commercial MOSFET Using a ZnO Nanowires Extended Gate. *IEEE Trans. Nanotechnol.* **2009**, *8*, 678−683.
(26) Zhu, Z.; Hattori, K.; Zhang, H.; Jimenez, X.; Ludwig, D. L.; Dias, S.; Kussie, P.; Koo, H.; Kim, H. J.; Lu, D.; Liu, M.; Tejada, R.; Friedrich, M.; Bohlen, P.; Witte, L.; Rafii, S. Inhibition of human leukemia in an animal model with human antibodies directed against vascular endothelial growth factor receptor 2. Correlation between antibody affinity and biological activity. *Leukemia* **2003**, *17*, 604−611.
(27) Igawa, T.; Ishii, S.; Tachibana, T.; Maeda, A.; Higuchi, Y.; Shimaoka, S.; Moriyama, C.; Watanabe, T.; Takubo, R.; Doi, Y.; Wakabayashi, T.; Hayasaka, A.; Kadono, S.; Miyazaki, T.; Haraya, K.; Sekimori, Y.; Kojima, T.; Nabuchi, Y.; Aso, Y.; Kawabe, Y.; Hattori, K. Antibody recycling by engineered pH-dependent antigen binding improves the duration of antigen neutralization. *Nat. Biotechnol.* **2010**, *28*, 1203−1207.
(28) Truneh, A.; Sharma, S.; Silverman, C.; Khandekar, S.; Reddy, M. P.; Deen, K. C.; McLaughlin, M. M.; Srinivasula, S. M.; Livi, G. P.; Marshall, L. A.; Alnemri, E. S.; Williams, W. V.; Doyle, M. L. Temperature-sensitive differential affinity of TRAIL for its receptors - DR5 is the highest affinity receptor. *J. Biol. Chem.* **2000**, *275*, 23319−23325.
(29) Gao, N.; Zhou, W.; Jiang, X.; Hong, G.; Fu, T.-M.; Lieber, C. M. General strategy for biodetection in high ionic strength solutions using transistor-based nanoelectronic sensors. *Nano Lett.* **2015**, *15*, 2143−2148.
(30) Kanai, Y.; Ohmuro-Matsuyama, Y.; Tanioku, M.; Ushiba, S.; Ono, T.; Inoue, K.; Kitaguchi, T.; Kimura, M.; Ueda, H.; Matsumoto, K. Graphene Field Effect Transistor-Based Immunosensor for Ultrasensitive Noncompetitive Detection of Small Antigens. *ACS Sens.* **2020**, *5*, 24−28.
(31) Kesler, V.; Murmann, B.; Soh, H. T. Going beyond the Debye Length: Overcoming Charge Screening Limitations in Next-Generation Bioelectronic Sensors. *ACS Nano* **2020**, *14*, 16194−16201.
(32) Nakatsuka, N.; Yang, K.-A.; Abendroth, J. M.; Cheung, K. M.; Xu, X.; Yang, H.; Zhao, C.; Zhu, B.; Rim, Y. S.; Yang, Y.; Weiss, P. S.; Stojanović, M. N.; Andrews, A. M. Aptamer-field-effect transistors overcome Debye length limitations for small-molecule sensing. *Science* **2018**, *362*, 319−324.

https://doi.org/10.1021/acssensors.2c00967
ACS Sens. 2022, 7, 2075−2083

(33) Liang, Y.; Xiao, M.; Wu, D.; Lin, Y.; Liu, L.; He, J.; Zhang, G.; Peng, L.-M.; Zhang, Z. Wafer-Scale Uniform Carbon Nanotube Transistors for Ultrasensitive and Label-Free Detection of Disease Biomarkers. *ACS Nano* **2020**, *14*, 8866−8874.
(34) Xiao, M.; Liang, S.; Han, J.; Zhong, D.; Liu, J.; Zhang, Z.; Peng, L. Batch Fabrication of Ultrasensitive Carbon Nanotube Hydrogen Sensors with Sub-ppm Detection Limit. *ACS Sens.* **2018**, *3*, 749−756.
(35) Song, S.; Wang, L.; Li, J.; Fan, C.; Zhao, J. Aptamer-based biosensors. *TrAC, Trends Anal. Chem.* **2008**, *27*, 108−117.
(36) Jayasena, S. D. Aptamers: An Emerging Class of Molecules That Rival Antibodies in Diagnostics. *Clin. Chem.* **1999**, *45*, 1628−1650.
(37) Chan, H.-N.; Xu, D.; Ho, S.-L.; He, D.; Wong, M. S.; Li, H.-W. Highly sensitive quantification of Alzheimer's disease biomarkers by aptamer-assisted amplification. *Theranostics* **2019**, *9*, 2939−2949.
(38) Bieschke, J.; Herbst, M.; Wiglenda, T.; Friedrich, R. P.; Boeddrich, A.; Schiele, F.; Kleckers, D.; Lopez del Amo, J. M.; Grüning, B. A.; Wang, Q.; Schmidt, M. R.; Lurz, R.; Anwyl, R.; Schnoegl, S.; Fändrich, M.; Frank, R. F.; Reif, B.; Günther, S.; Walsh, D. M.; Wanker, E. E. Small-molecule conversion of toxic oligomers to nontoxic beta-sheet-rich amyloid fibrils. *Nat. Chem. Biol.* **2011**, *8*, 93−101.
(39) Karran, E.; Mercken, M.; Strooper, B. D. The amyloid cascade hypothesis for Alzheimer's disease: an appraisal for the development of therapeutics. *Nat. Rev. Drug Discovery* **2011**, *10*, 698−712.
(40) White, R. J.; Phares, N.; Lubin, A. A.; Xiao, Y.; Plaxco, K. W. Optimization of Electrochemical Aptamer-Based Sensors via Optimization of Probe Packing Density and Surface Chemistry. *Langmuir* **2008**, *24*, 10513−10518.
(41) Zheng, Y.; Geng, X.; Yang, X.; Li, S.; Liu, Y.; Liu, X.; Wang, Q.; Wang, K.; Jia, R.; Xu, Y. Exploring Interactions of Aptamers with $A\beta_{40}$ Amyloid Aggregates and Its Application: Detection of Amyloid Aggregates. *Anal. Chem.* **2020**, *92*, 2853−2858.

https://doi.org/10.1021/acssensors.2c00967
ACS Sens. 2022, 7, 2075−2083